AIAA JOURNAL
Vol. 32, No. 4, April 1994

Compressible Turbulence Measurements in a High-Speed High-Reynolds-Number Mixing Layer

Rodney D. W. Bowersox*
Air Force Institute of Technology, Wright-Patterson Air Force Base, Ohio 45433
and
Joseph A. Schetz†
Virginia Polytechnic Institute and State University, Blacksburg, Virginia 24061

To assess the significant physics associated with compressible turbulence, extensive multiple overheat cross/normal-wire, shadowgraph image processing and conventional probe surveys were obtained in a two-dimensional, supersonic, free mixing layer, which consisted of Mach 1.8 air (Re/m = 7 × 10⁶) injected tangentially into a Mach 4.0 freestream (Re/m = 67 × 10⁶). A turbulence transformation was developed that allowed direct measurement of the total Reynolds shear stress. Profiles of three-dimensional turbulent shear, apparent mass, and heat flux data were acquired. Compressibility was found to account for 75% of the total compressible Reynolds shear stress (i.e., the incompressible term, $\overline{\rho u'v'}$, accounted for only 25%) and 100% of the turbulent heat flux in the present nominally adiabatic flow. These data allowed the development and experimental evaluation of various turbulence closure formulations. The incompressible models yielded results consistent with measured incompressible terms. The Situ-Schetz compressible model accurately represented the total shear. However, the present data indicated that this model provided poor estimates of the turbulent heat flux. Hence, the Situ-Schetz techniques were generalized to consistently account for compressibility in all of the conservation equations. The performance of the new model was found to be excellent. New compressible turbulent kinetic energy formulations were also developed and evaluated.

Nomenclature

A	=	hot-wire angle sensitivity
B	=	shear layer width
a, b	=	hot-wire calibration constants
G	=	single-sided frequency spectra
H	=	slot exit height
h	=	film contrast
K	=	Gladstone-Dale constant
k	=	thermal conductivity
M	=	Mach number
Nu	=	Nusselt number
P, p	=	pressure
Pr	=	Prandtl number
q	=	heat flux
Re	=	Reynolds number
T	=	temperature
TKE	=	turbulent kinetic energy
u, v, w	=	velocity components
x, y, z	=	Cartesian coordinates
α, β	=	$f(M)$
γ	=	ratio of specific heats
Δ	=	shadowgraph sensitivity
δ	=	boundary-layer thickness
μ	=	viscosity
ρ	=	density
σ	=	variance
τ	=	shear stress
ϕ	=	hot-wire incidence angle

Subscripts

c	=	compressible
e	=	effective
n	=	normal component
s	=	slot
T	=	turbulent
t	=	total condition or tangential component
w	=	wire or wall
o	=	reference condition

Superscripts

T	=	turbulent
$( )'$	=	fluctuating component
$\overline{( )}$	=	mean component

Introduction

TURBULENCE modeling remains the controlling factor in the accuracy of all high-speed, high-Reynolds-number computational boundary-layer and Navier-Stokes predictions. The current focus on hypersonic flight, coupled with the fact that most of the prior fundamental work on turbulence modeling has been for incompressible flows, requires that compressible turbulence modeling be directly addressed. The most common approach to Navier-Stokes predictions is based on either the classical Reynolds- (time-) averaged or the Favre- (mass-weighted-time) averaged Navier-Stokes equations.[1,2] Closure formulations (turbulence models) are needed for both averaging methods.

Experimental information is crucial in the development of turbulence models that are to incorporate the significant flow physics. Liou and Shih[1] suggest that the Favre-averaged equations perform poorly for free shear layers and in the presence of shock waves and expansion fans; hence the present study concentrates on the Reynolds-averaged formulation. For thin layer type flows, in addition to the usual incompressible terms, compressible turbulence manifests itself in each of the governing equations through an apparent mass. Situ and Schetz[2] accounted for the apparent mass in the Reynolds shear stress

Presented as Paper 93-0660 at the AIAA 31st Aerospace Sciences Meeting, Reno, NV, Jan. 11–14, 1993; received March 10, 1993; revision received Oct. 18, 1993; accepted for publication Oct. 26, 1993.

*Assistant Professor, Department of Aerospace Engineering. Member AIAA.
†J. Byron Maupin Professor, Department of Aerospace and Ocean Engineering. Fellow AIAA.

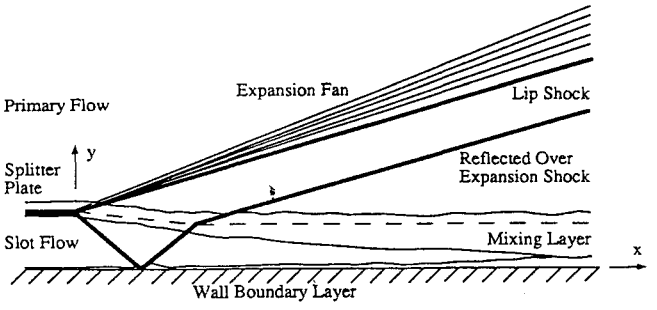

Fig. 1 Flowfield schematic.

by invoking a gradient transport compressible mixing length formulation. The present study generalizes this idea to each of the conservation equations (i.e., continuity, momentum, and energy). The new compressible apparent mass mixing length extension (CAMMLE) model, which is a further extension of the original Prandtl and Situ-Schetz mixing length formulations, was experimentally validated. In addition, the definition of a new compressible turbulent kinetic energy (TKE_c) allowed logical extensions of the Prandtl and Bradshaw TKE formulations.

To measure compressible turbulence, some innovative experimental techniques had to be developed. A turbulence transformation was developed that allowed the direct measurement of the compressible Reynolds shear stress via cross-wire anemometry, shadowgraph image processing, and conventional mean flow probes.

As discussed by Hyde et al.,[3] studies that include both mean and turbulence quantities are rare. In addition, compressible turbulent shear data are practically nonexistent. A supersonic free mixing layer (see Fig. 1) was chosen here to study compressible turbulence. The main advantage of this flow is that the effects of compressibility become significant at lower Mach numbers compared with wall-bounded flows.[4] Possible practical interests for this flow include surface cooling, skin friction reduction, and Scramjet fuel injection. The experimental flowfield can be considered a near full-scale ideal model Scramjet combustor, consisting of Mach 1.8 (Re/m = 7 × 10^6) air tangentially injected into a Mach 4.0 freestream (Re/m = 67 × 10^6), separated by a turbulent free shear layer. The "combustor" freestream Mach number is typical for aircraft flight Mach numbers of 8–16.

In this paper, the compressible turbulence terms in the Reynolds-averaged form of the governing equations will be written in a form that is both experimentally and numerically convenient. New experimental techniques are developed to allow the direct measurement of the total compressible Reynolds shear. Detailed three-dimensional surveys of the compressible shear, apparent mass, and heat flux data at four measurement stations were acquired. Since this paper is a turbulence study, only the results at a single station (x/H = 15) will be presented here (remaining data can be found in Bowersox[5]). These data allowed the development of new turbulence models. The new models as well as existing incompressible and compressible formulations are experimentally evaluated.

Turbulence Analysis

The compressible, conservative form, Reynolds-averaged, Navier-Stokes equations written in Cartesian coordinates are given by

$$\frac{\partial \bar{\rho}}{\partial t} + \frac{\partial}{\partial x_j}(\bar{\rho}\bar{u}_j + \overline{\rho' u_j'}) = 0$$

$$\frac{\partial}{\partial t}(\bar{\rho}\bar{u}_i + \overline{\rho' u_i'}) + \frac{\partial}{\partial x_j}(\bar{\rho}\bar{u}_i\bar{u}_j) = -\frac{\partial \bar{p}}{\partial x_i} + \frac{\partial}{\partial x_j}(\tau_{ij} + \tau_{ij}^T) \quad (1)$$

$$\frac{\partial}{\partial t}(\bar{\rho}\bar{e}_0 + \overline{\rho' h_0'}) + \frac{\partial}{\partial x_j}(\bar{\rho}\bar{h}_0\bar{u}_j) = \frac{\partial}{\partial x_j}(\bar{u}_i\bar{\tau}_{ij} + \overline{u_i'\tau_{ij}'} - q_j - q_j^T)$$

where the compressible turbulence terms can be written as

$$m_i^T = -\overline{\rho' u_i'}$$

$$\tau_{ij}^T = -\bar{\rho}\overline{u_i' u_j'} - \bar{u}_i\overline{\rho' u_j'} - \bar{u}_j\overline{\rho' u_i'} - \overline{\rho' u_i' u_j'} \quad (2)$$

$$q_i^T = +\bar{\rho}\overline{h_0' u_i'} + \bar{h}_0\overline{\rho' u_i'} + \bar{u}_i\overline{\rho' h_0'} + \overline{\rho' h_0' u_i'}$$

The turbulent apparent mass m^T, compressible shear τ^T, and compressible heat flux q^T terms are associated with the continuity, momentum, and energy equations, respectively. For incompressible flows, the apparent mass and the last three terms in the shear stress and heat flux are zero. For compressible, thin layer flows, where x is denoted as the axial coordinate and y the transverse, the expressions in Eq. (2) reduce to

$$m_y^T = -\overline{\rho' v'} \quad (3a)$$

$$\tau_{xy}^T = -\bar{\rho}\overline{u' v'} + \bar{u} m_y^T \quad (3b)$$

$$q_y^T = +\bar{\rho}\overline{h_0' v'} - \bar{h}_0 m_y^T \quad (3c)$$

As can be seen in Eq. (3), compressibility manifests itself through the y component of apparent mass. Unfortunately, little data exist to determine the relative importance of each of the terms in Eq. (3).

Turbulence Transformation

The apparent mass terms cannot be directly measured. Therefore, the shear stress and heat flux in Eq. (2) were transformed using the following identity,

$$\begin{aligned}\rho\phi &= \overline{\rho\phi} + (\rho\phi)' \\ &= \bar{\rho}\bar{\phi} + \bar{\rho}\phi' + \bar{\phi}\rho' + \rho'\phi'\end{aligned} \quad (4)$$

where ϕ is a generic variable. With Eq. (4), Eq. (2), neglecting third-order terms, can be rewritten as

$$\tau_{ij}^T = -\frac{\overline{(\rho u_i)'(\rho u_j)'}}{\bar{\rho}} + \bar{\rho}\bar{u}_i\bar{u}_j\overline{\left(\frac{\rho'}{\bar{\rho}}\right)^2} \quad (5a)$$

$$q_i^T = +\bar{\rho}\overline{(\rho u_i)' h_0'} + \bar{h}_0\overline{\rho' u_i'} \quad (5b)$$

All of the second-order terms, except the apparent mass in the second heat flux term, in Eq. (5) can be directly measured with the cross-wire, shadowgraph processing, and the conventional mean flow probes.[5] The apparent mass term can be estimated by "separating" the cross-wire variables.

Turbulence Models

All incompressible turbulent shear stress models only account for the first term in Eq. (3b).[6] Most compressible models are based on ad hoc extensions of incompressible ones.[6] However, simply allowing the density to vary or "re-tuning" model constants does not rigorously account for compressibility. Situ and Schetz[2] extended the incompressible Prandtl mixing length model to compressible flows by introducing a mixing length formulation that includes the second term in the compressible shear stress formulation [Eq. (3b)]. Since compressible shear data are very scarce, Situ and Schetz[2] were unable to directly validate their turbulence formulation. However, their model did produce improved numerical mean flow predictions for both two-dimensional wall boundary and free mixing layers.[2]

Situ and Schetz,[2] as well as most other researchers, treat the energy equation turbulence through an ad hoc effective turbulent eddy viscosity and a constant turbulent Prandtl number to yield an eddy thermal conductivity. To be specific, even for compressible flows, the second term in the turbulent

heat flux [Eq. (3)] is usually neglected, and the first term is expanded into nonconservative form (i.e., into the static enthalpy and velocities). Then the typical incompressible effective eddy viscosity and constant turbulent Prandtl number formulations are used.[6] Clearly, if the apparent mass term is significant in the shear stress formulation, it should also be included in the energy and continuity equations. Hence, the present study proposes to extend this notion further to each apparent mass term in Eq. (3).

The new CAMMLE model is given by

$$m_y^T = \left|\frac{\partial \bar{\rho}}{\partial y}\right| \frac{\partial \bar{u}}{\partial y} \frac{L_m^2}{S} \tag{6a}$$

$$\tau_{xy}^T = \mu_T \frac{\partial \bar{u}}{\partial y} + \bar{u} m_y^T \tag{6b}$$

$$q_y^T = -\frac{\bar{\rho}}{Pr_T} \left|\frac{\partial \bar{u}}{\partial y}\right| \frac{\partial \overline{h_0}}{\partial y} L_m^2 - \overline{h_0} m_y^T \tag{6c}$$

where μ_T is the original Prandtl mixing length eddy viscosity (i.e., $\mu_T = L_m^2 \bar{\rho} |\partial \bar{u}/\partial y|$), and the key step in the compressible turbulence modeling is taking $\rho' \sim (L_m/S)|\partial \bar{\rho}/\partial y|$. The CAMMLE shear stress formulation [Eq. (6b)] is very similar to that of Situ and Schetz,[2] where the only difference is that the absolute values are slightly redefined. The CAMMLE turbulent heat flux model [Eq. (6c)] deviates from the normal eddy thermal conductivity procedure, as discussed earlier; instead, Eq. (3c) was modeled in a gradient transport fashion consistent with the compressible shear approach. As will be seen later, this results in a significant improvement. The accepted incompressible conventions are incorporated to determine the mixing length values.[4,6] Situ and Schetz[2] set the new constant S equal to the turbulent Schmidt number via a turbulent diffusion analogy. Li and Nagamatsu,[7] in an effort to determine a compressible skin friction law, defined a wall shear formulation similar to that in Eq. (6), where they proposed the new constant to be a function of Mach number (i.e., for boundary layers, as $M \to 0$, $1/S \to 0$ and as $M \to \infty$, $1/S \to 1$). Bushnell and Beckwith[8] also incorporated a density fluctuation term in their formulation of the compressible shear stress, and in that study S was set to 1.0 (by definition). The present study defines S, for free shear layers, via a compressible extension of the Prandtl energy model and the present data.

The Prandtl and Bradshaw turbulent kinetic energy shear stress models were also developed based on incompressible data.[6] The present study proposes to generalize these models by introducing the "compressible" turbulent kinetic energy (TKE_c), which is given by

$$TKE_c = \frac{\overline{(\rho u)'^2} + \overline{(\rho v)'^2} + \overline{(\rho w)'^2}}{2\bar{\rho}^2} \tag{7}$$

The CAMMLE shear stress formulation can be derived from the Prandtl energy model evaluated with TKE_c, and based on this exercise S was set to unity.[5] The new compressible formulations, as well as various incompressible models, were experimentally tested.

It should also be noted that each of the compressible models developed here reduces to the corresponding incompressible formulations for constant density or low Mach number flows.

Experimental Apparatus

Facilities

All tests were performed in the Virginia Tech supersonic wind tunnel. This blowdown facility provided run times of about 9 s at a freestream Mach number of 4.0. The settling chamber pressure $P_{t\infty}$ and temperature were nominally 12.5 atm and 295 K, yielding a freestream Re/m of 67×10^6. The test section was 23 cm wide, 14 cm high, and 51 cm long.

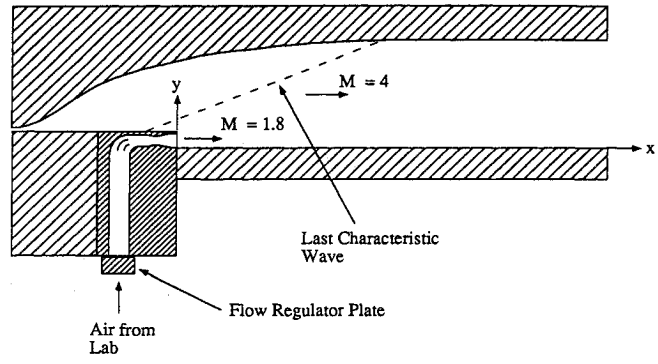

Fig. 2 Sketch of the wind tunnel and injection model configuration.

The injection model was built into the Mach 4.0 nozzle as shown in Fig. 2. The slot Mach number was designed to be 1.8. The slot total pressure and temperature were nominally 0.52 atm and 297 K, producing an Re/m of 7×10^6. The exit height H was 2.54 cm.

Instrumentation

Conventional pitot and cone-static pressure profiles were made at each of the four axial measurement stations. The Mach number was computed from the ratio of the cone-static pressure to the pitot pressure.

Constant temperature anemometer systems were used with normal-wire and cross-wire probes. Transistor-Transistor Logic circuitry was developed to rapidly change the wire temperature.[5] Eight overheat resistance values were scanned. Therefore, a least-squares analysis was applied to reduce errors.[9] The maximum overheat ratio (or resistance ratio) was 2.1, and the minimum was about 1.35.

The wind-tunnel facility is equipped to take both nanosecond shadowgraphs and microsecond spark schlierens. For the present study, shadowgraphs were taken. The light was passed through the test section through large optical grade Plexiglas windows onto a photographic plate that was nominally 0.40 m from the center of the test section. The film used in the study was Polaroid Type 57.[10] The shadowgraphs were digitized into gray scales, and the gray scales were converted into film exposure E.

Data Reduction

Mach number profiles were computed from the ratio of pitot and cone-static pressure. Error analysis indicates that the results are accurate to ± 0.1.

Multiple overheat, supersonic normal-wire anemometry has received a great deal of attention.[3,9,11] However, supersonic cross-wire anemometry has received only moderate concentration. The methods of Demetriades and Laderman[12] exemplify the current use of supersonic cross-wire anemometry. The present analysis generalizes the normal-wire techniques to include cross-wire methods by introducing an effective Reynolds number concept for compressible flows, which is similar to the incompressible effective velocity presented by Champagne et al.[13] This interpretation, as will be seen, yields the first term in Eq. (5). Error analysis[5] indicates that the turbulence intensity and correlation errors are about 5 and 10%, respectively.

The Nusselt number, the dimensionless heat transfer, of a cylinder can be empirically related to the Reynolds number by[9]

$$Nu = a\sqrt{Re_e} + b \tag{8}$$

The Nusselt number is also proportional to the wire power {i.e., $Nu = q_w/[\pi k_f L(T_w - T_f)]$}, which implies that the squared hot-wire voltage is proportional to the square root of the

effective Reynolds number and the total temperature. To obtain the mean and fluctuation equations, we replaced the voltage, Reynolds number, and total temperature by their mean and fluctuating component, and the binominal theorem was applied.[5,9]

To arrive at the cross-wire results, the effective Reynolds number must be related to the x and y components in tunnel axes (see Fig. 2 for the coordinate system definition). The analysis presented here will parallel the end loss correction technique of Champagne et al.[13] with the addition of oblique shock theory. Thus,

$$\begin{aligned} Re_e^2 &= Re_n^2 + k_c^2 Re_t^2 \\ &= A_1 Re_x^2 + 2A_2 Re_x Re_y + A_3 Re_y^2 \end{aligned} \tag{9}$$

where the various A_i are given by

$$\begin{aligned} A_1 &= \cos^2(\phi) + k_c^2 \sin^2(\phi) \\ A_2 &= (1 - k_c^2)\cos(\phi)\sin(\phi) \\ A_3 &= k_c^2 \cos^2(\phi) + \sin^2(\phi) \end{aligned} \tag{10}$$

The determination of k_c stems from Champagne et al. and the oblique shock theory. After making first-order assumptions, one can show $k_c = \bar{\rho}_1/\bar{\rho}_2 k$, where 1 refers to conditions just before the oblique shock preceding the wire, 2 refers to the conditions behind the oblique shock, and k is to be determined experimentally. Here, the result of Spangenberg,[14] where $Re_e = Re_n$ (i.e., $k_c = 0$), was applied. This will yield minimal error if the wires are calibrated at flow angles close to those expected in the flow.

Replacing the effective Reynolds number and the x and y components by the mean and fluctuating parts, one can show that

$$\overline{Reo_{ej}} = \overline{Reo_x}\sqrt{B_{3j}} \tag{11a}$$

$$\left(\frac{Reo_e'}{\overline{Reo_e}}\right)_j = B_{1j}\left(\frac{Reo_x'}{\overline{Reo_x}}\right) + B_{2j}\left(\frac{Reo_y'}{\overline{Reo_x}}\right) \tag{11b}$$

where $R_0 = \overline{\rho v}/\overline{\rho u}$, $B_1 = A_1/B_3$, $B_2 = A_2/B_3$, $B_3 = A_1 + 2A_2R_0$, and j indexes the cross-wire sensors on the probe. In the derivation of Eq. (11) it was assumed that $R_0^2 < 1$. The mean results, in the tunnel coordinate system, can be obtained by solving Eq. (11a). The turbulence results can be transformed into x and y components by solving Eq. (11b).

The x and y Reynolds number total temperature correlations can also be resolved. To measure turbulence in the x-z plane, the cross-wire probe was rotated by 90 deg, v was replaced by w, and y was replaced by z.

To decompose the conservative cross/normal-wire results into nonconservative variables, the assumption that $p' \approx 0$ was invoked. The relations between the variables can be expressed as

$$\begin{aligned} \frac{u'}{\bar{u}} &= \frac{(\rho u)'}{\overline{\rho u}} - \frac{\rho'}{\bar{\rho}} \\ \frac{v'}{\bar{u}} &= \frac{(\rho v)'}{\overline{\rho u}} - R_0\frac{\rho'}{\bar{\rho}} \\ \frac{\rho'}{\bar{\rho}} &= \frac{1}{\alpha + \beta}\left\{\beta\left[\frac{(\rho u)'}{\overline{\rho u}} + R_0\frac{(\rho v)'}{\overline{\rho u}}\right] - \frac{T_t'}{\bar{T}_t} + \alpha\frac{p'}{\bar{p}}\right\} \end{aligned} \tag{12}$$

where $\alpha = [1 + \frac{1}{2}(\gamma - 1)M^2]^{-1}$ and $\beta = (\gamma - 1)\alpha M^2$. With Eq. (12) and neglecting the p' term, one can arrive at all of the turbulence shear terms in the Reynolds-averaged formulation, Eq. (2). However, the assumption of $p' = 0$ remains problematical. Kistler[15] suggests that p' is proportional to u'^2; thus it is second order. Referring to the density fluctuation equation in Eq. (12), the effects of p' can be seen. It is important to notice that p' is multiplied by α, which is always less than 1 [$\alpha \in (0.24, 0.66)$ for the $M \in (1.6, 4.0)$]. Thus, even if p' is not zero, perhaps the effects on the cross-wire response are still small. Results will be presented both with and without this assumption.

The shadowgraph analysis, presented here, parallels the schlieren methods of Clay et al.[16] The fluctuation film contrast [$h = (E - E_0)/E$] of the shadowgraph can be related to the index of refraction by[17]

$$h' = L\int_0^W \left(\frac{\partial^2 n'}{\partial x^2} + \frac{\partial^2 n'}{\partial y^2}\right) dz \tag{13}$$

where L is the distance from the centerline of the test section to the film plate and W is the width of the test section. The variable L was made as small as possible to insure one-to-one correspondence between the index of refraction field and the shadowgraph. Taking the autocorrelation (in two dimensions) of Eq. (13) and also taking advantage of the inherent averaging across the test section, one can show that the density fluctuation variance can be expressed as

$$\sigma_\rho^2 = \frac{1}{\Delta}\int_0^\infty\int_0^\infty \frac{G_{hh}(f_x, f_y)}{f_x^4 + f_y^4}\, df_x\, df_y \tag{14}$$

where G_{hh} is the two-dimensional single-sided autospectra function of the fluctuation film contrast, and $\Delta = 4.37(2\pi)^4(KLW)^2$, where K is the Gladstone-Dale constant ($=2.38 \times 10^{-4}$ m^3/kg for air). The assumptions in arriving at Eq. (14) are consistent with those of Clay et al.,[16] except that Clay assumed that the density fluctuation field was isotropic. That assumption was not necessary here.

Results and Discussion

Shadowgraph

Figure 3 presents the composite shadowgraph, where the flow is from right to left, and the injection is along the lower floor. The freestream boundary-layer thickness ($\delta_\infty = 4.5$ mm), near the lip of the injector, the lip and the slot overexpansion shocks, the turbulence eddy structure, and the shear layer spreading rate (≈ 0.03) are clearly visible on the shadowgraph.

Mean Flow Data

Detailed data profiles were acquired at each of the four stations marked on Fig. 3. Figure 4 shows the Mach number

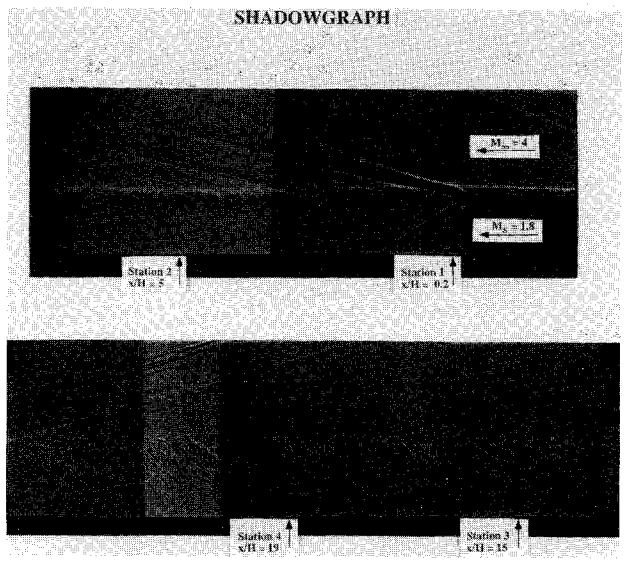

Fig. 3 Composite shadowgraph; flow is from left to right, and the injection is along the lower floor.

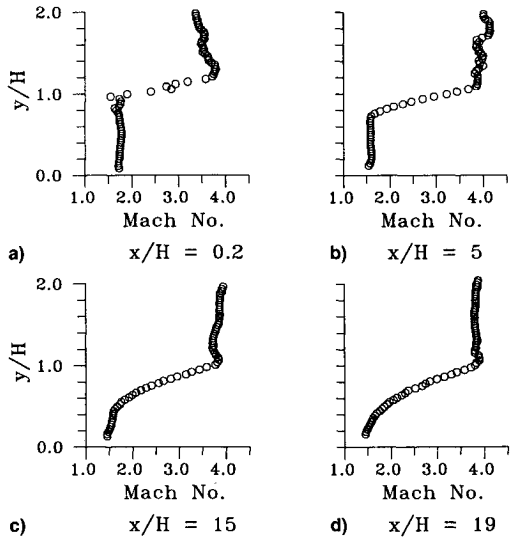

Fig. 4 Mach number profiles at the four measurement stations.

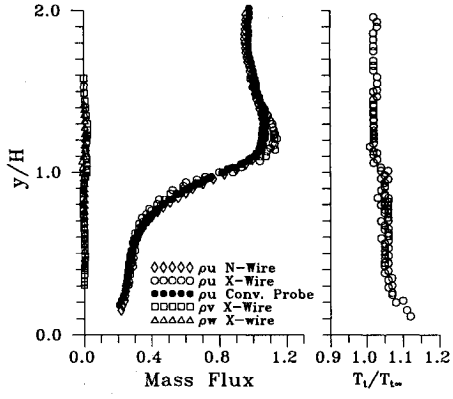

Fig. 5 Mean mass flux and total temperature at x/H = 15; profiles normalized by the local freestream value.

profiles at the four stations measured with the conventional mean flow probes. The growth of the mixing layer and lower wall boundary layer is evident in the figure. The smoothly increasing profiles, from x/H = 5 to 19, indicate that the shear layer is fully developed in this region.[4] The spreading rate, db/dx, was estimated at about 0.028. The shear layer and floor boundary layer merged by the last station. Since this paper is intended as a turbulence study, the remaining data will be restricted to station 3 (i.e., detailed flowfield mapping is not the goal of the paper). See Bowersox[5] for complete data at the remaining stations.

Figure 5 gives the mean mass flux and total temperature profile results. The y and z components of mass flux are essentially zero. The x component was measured with a variety of probes ("N-Wire" denotes normal wire, "X-Wire" denotes cross wire, "Conv. Probe" denotes conventional mean flow probes). The excellent agreement between the measurement techniques yields confidence in both the flow repeatability and probe accuracy. Error analysis implies a ±2% confidence interval. The total temperature profile measured with the cross-wire and normal-wire probes indicates that the injection total temperature was about 3% higher than that of the freestream.

Turbulence Data

Figure 6 presents the turbulence intensity data obtained with the cross-wire and normal-wire probes, in both cross/normal-wire and separated variables. As can be seen in the cross-wire results, the axial mass flux turbulence intensity is the largest. The transverse and spanwise mass flux turbulence intensities are about the same at 80% of the axial value. The total temperature turbulence intensity was about 2% in this

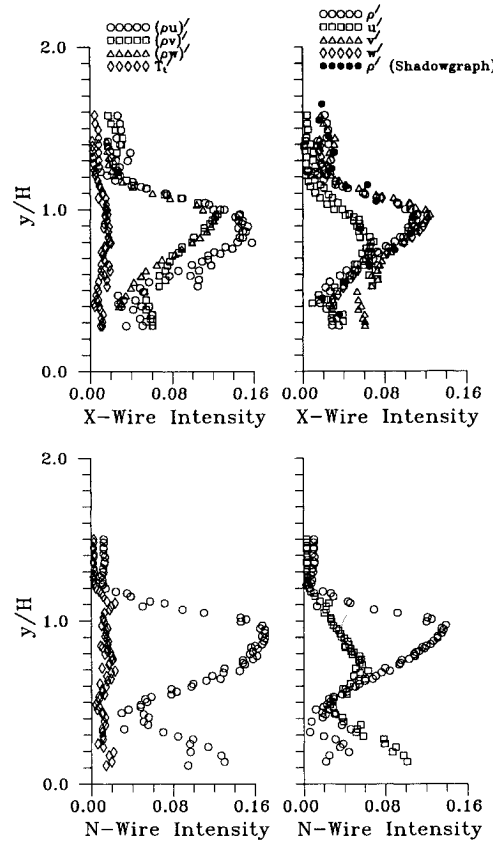

Fig. 6 Root-mean-square turbulence intensity at x/H = 15; profiles normalized by the local mean value.

nominally constant mean total temperature flow. The shadowgraph density fluctuation results are included in the cross-wire separated turbulence intensity plot. The agreement between the two techniques is considered excellent, yielding confidence in both methods. It is also interesting to note that the separated transverse (v') and spanwise (w') velocity fluctuations are essentially identical at about twice the axial level. The density fluctuations are also about twice those of the axial velocity.

The normal-wire probe was able to traverse much closer to the test section wall; hence these results are included. An important trend reversal phenomenon can be seen in the separated normal-wire results. In the wall boundary layer, the velocity fluctuation levels are about twice those of the density. However, immediately upon traversing into the free mixing layer, the trend is reversed (i.e., the density turbulence intensity grows to about 2.5 times that of the velocity intensity). The turbulence intensity results are important in determining the structure of the flowfield; however, they provide no direct turbulence modeling information.

The cross-wire shear data are presented in Fig. 7. As can be seen, the first term in Eq. (5) is the only significant term for thin layer type flows (i.e., $\bar{v}$ is small). Figure 8 gives the Reynolds shear stress results. One can note that the apparent mass component accounts for about 75% of the total level of the shear.

The turbulent heat flux results are given in Fig. 9. The axial component is the largest, which may explain the reported difficulties with the Favre-averaged computational fluid dynamics (CFD) approach.[1] Recall that the y component is the important term for thin layer, Reynolds-averaged flows [Eq. (3c)]. Since $\bar{v}$ is very small, the mass flux total temperature correlation is essentially the incompressible term in Eq. (3c). The y component term is seen to be essentially zero.

Turbulence Modeling

The estimated y component of apparent mass, along with a prediction from the CAMMLE model formulation [Eq. (6)

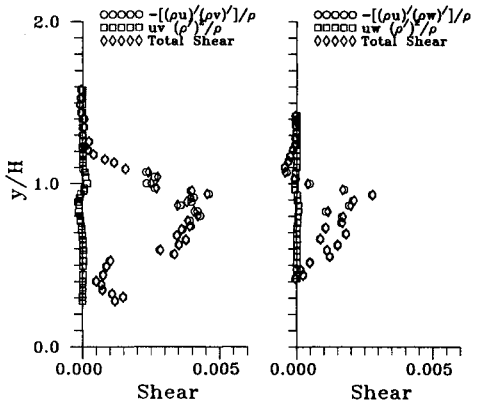

Fig. 7 Compressible turbulent shear stress in transformed (cross-wire) variables at $x/H = 15$; profiles normalized by axial local mean values.

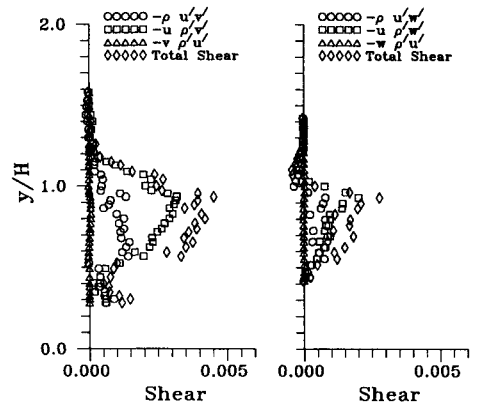

Fig. 8 Reynolds shear stress components at $x/H = 15$; profiles normalized by axial local mean values.

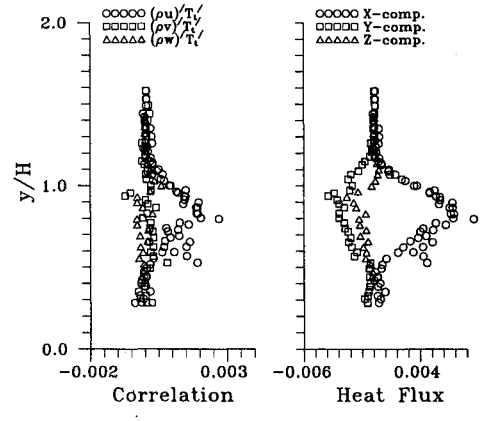

Fig. 9 Mass flux total temperature correlations and compressible turbulent heat flux components; both profiles normalized by axial local mean values.

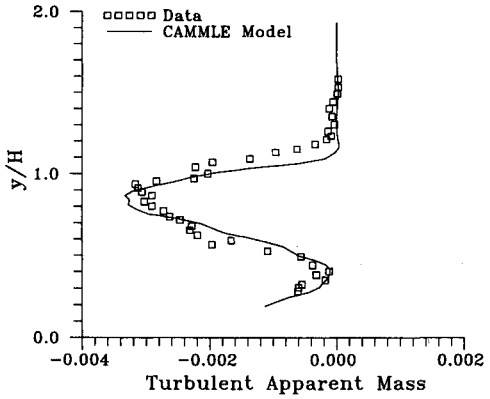

Fig. 10 Compressible turbulent apparent mass data and CAMMLE model results (evaluated with the measured data) at $x/H = 15$; profiles normalized by local axial mean values.

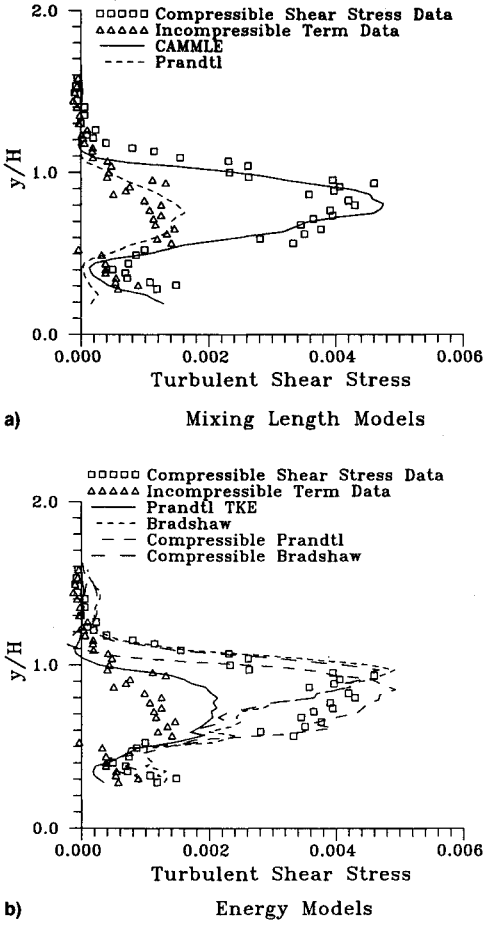

Fig. 11 Turbulent shear stress data and model results (evaluated with the measured data) at $x/H = 15$; profiles normalized by local axial mean values.

evaluated with the mean flow data], is given in Fig. 10. The agreement with apparent mass expression in Eq. (6) is considered excellent. Note that the typical incompressible value of L_m ($=0.07B$, where B is the layer width[18]) was adopted,[4] and S was set to 1.0, $B/H = 0.66$ at this station.

Figures 11a and 11b present the full compressible Reynolds shear stresses, Eq. (5a), and the estimated incompressible term [the first term in Eq. (3b)]. The incompressible Prandtl mixing length model [the first term in Eq. (6b)] performs very well in estimating the incompressible part of the shear stress. The agreement between the CAMMLE model [the full shear stress formulation in Eq. (6b)] and the data is again excellent (Fig. 11a). The incompressible Prandtl energy model, evaluated with typical incompressible model constants,[6] also performs well at estimating the incompressible shear term (Fig. 11b). Surprisingly, the incompressible Bradshaw method, evaluated with the typical incompressible model constants,[6] agrees with the total compressible shear. The compressible energy extensions [evaluated with TKE_c defined in Eq. (7)] also produce accurate results. However, the Prandtl TKE proportionality constant was set to unity, and the Bradshaw model constant was reduced to 0.18. The changes allowed better agreement with the measured data.

Figure 12 presents estimates of the turbulent heat flux [Eq. (5b)]. One can see that the first term in Eq. (3c) is nominally zero; however, the compressible apparent mass term is not small in this nominally constant total temperature flow. The CAMMLE model performs very well in estimating the total heat flux [Eq. (6c)]. The incompressible effective eddy vis-

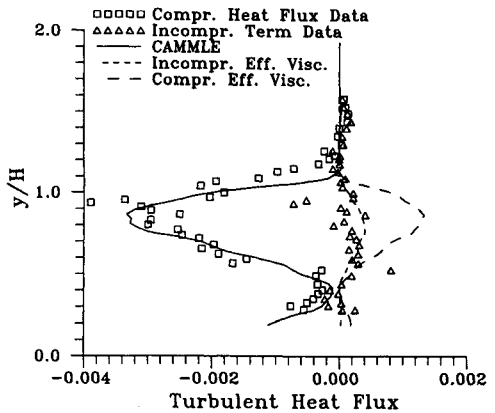

Fig. 12 Turbulent heat flux data and model results (evaluated with the measured data) at $x/H = 15$; profiles normalized by local axial mean values.

cosity and constant Prandtl number methods provide accurate estimates of the incompressible part of the heat flux data. However, the normal ad hoc compressible effective viscosity and constant turbulent Prandtl number formulations produce poor predictions of the compressible heat flux.

Conclusions

The most important conclusion to be made is that compressibility dominated the turbulence levels, accounting for 75% of the Reynolds shear and 100% of the turbulent heat flux for this flow, which had a nearly constant total temperature distribution. For thin layer flows, compressibility manifests itself in each of the governing conservation equations (continuity, momentum, and energy) through the y component of apparent mass ($\rho' v'$). The new turbulence transformation developed here allowed consistent, inexpensive, and accurate measurement of the full compressible Reynolds shear. Multiple overheat cross-wire anemometry was shown to be a powerful compressible turbulence research tool. Incompressible turbulence models were found to provide accurate estimates of the incompressible part of the turbulent shear stress, and the Situ-Schetz compressible mixing length model, as well as the new TKE_c formulations, provided accurate estimates of the full compressible turbulent shear stress. Also, the commonly used effective eddy viscosity and constant turbulent Prandtl number assumption to account for the turbulent heat flux was found to be an inaccurate representation of the flow physics. Hence, the new methodology associated with the compressible apparent mass mixing length extension (CAMMLE) model was developed here, and that formulation accurately represented the compressible turbulence in all of the conservation equations.

References

[1]Liou, W. W., and Shih, T. H., "On the Basic Equations for the Second-Order Modeling of Compressible Turbulence," NASA TM 105277, Oct. 1991.

[2]Situ, M., and Schetz, J., "New Mixing Length Model for Turbulent High Speed Flows," *AIAA Journal*, Vol. 29, No. 6, 1991, pp. 872, 873.

[3]Hyde, R., Smith, B., Schetz, J., and Walker, D., "Turbulence Measurements for Heated Gas Slot Injection in Supersonic Flow," *AIAA Journal*, Vol. 28, No. 9, 1990, pp. 1605–1614.

[4]Bradshaw, P., "Compressibility Effects on Free-Shear Layers," in Kline, S., Cantwell, B., and Lilley, G., *The 1980–81 AFOSR-HTTM-Stanford Conference on Complex Turbulent Flows: Comparison of Computation and Experiment*, Vol. I, Stanford Univ. Press, Stanford, CA, 1981.

[5]Bowersox, R. D. W., "Compressible Turbulence in a High Speed High Reynolds Number Mixing Layer," Ph.D. Dissertation, Virginia Polytechnic Inst. and State Univ., Aerospace Engineering Dept., Blacksburg, VA, Sept. 1992.

[6]Schetz, J. A., *Boundary Layer Analysis*, Prentice-Hall, Englewood Cliffs, NJ, 1993.

[7]Li, T. Y., and Nagamatsu, H. T., "Effects of Density Fluctuations on the Turbulent Skin Friction of an Insulated Flat Plate at High Supersonic Speeds," *Journal of Aeronautical Sciences*, Vol. 18, June 1951, pp. 696–697.

[8]Bushnell, D. M., and Beckwith, I. E., "Calculation of Nonequilibrium Hypersonic Turbulent Boundary Layers and Comparisons with Experimental Data," *AIAA Journal*, Vol. 8, No. 8, 1970, pp. 1462–1469.

[9]Kovasznay, L. S. G., "The Hot-Wire Anemometer in Supersonic Flow," *Journal of Aeronautical Sciences*, Vol. 17, Sept. 1950, pp. 565–584.

[10]Polaroid High Speed Film Type 57, Data Sheet, PP479, Polaroid Corp., Cambridge, MA, March 1983.

[11]Bowersox, R. D. W., Ng, W., and Schetz, J., "Hot-Wire Techniques Evaluated in the Wake of a 2-D Supersonic Compressor Cascade," *Yokohama International Gas Turbine Congress*, Vol. 84, No. 3, 1991, pp. 303–309.

[12]Demetriades, A., and Laderman, J., "Reynolds Stress Measurements in a Hypersonic Boundary Layer," *AIAA Journal*, Vol. 11, No. 11, 1974, pp. 1594–1596.

[13]Champagne, F. H., Sleicher, C. A., and Wehrmann, O. H., "Turbulence Measurements with Inclined Hot-Wires," *Journal of Fluid Mechanics*, Vol. 28, Pt. 1, June 1966, pp. 153–175.

[14]Spangenberg, W. G., "Heat-Loss Characteristics of Hot-Wire Anemometers at Various Densities in Transonic and Supersonic Flow," NACA TN 3381, May 1955.

[15]Kistler, A., "Fluctuation Measurements in a Supersonic Turbulent Boundary Layer," *Physics of Fluids*, Vol. 2, No. 3, 1959, p. 290–296.

[16]Clay, W. G., Herrmann, J., and Slattery, R. E., "Statistical Properties of the Wake Behind Hypervelocity Spheres," *Physics of Fluids*, Vol. 8, No. 10, 1965, pp. 1792–1801.

[17]Kovasznay, L. S. G., "Optical Techniques," *Physical Measurements in Gas Dynamics and Combustion*, Princeton Univ. Press, Princeton, NJ, 1954, pp. 277–285.

[18]Launder, B. E., and Spalding, D. P., *Mathematical Models of Turbulence*, Academic Press, New York, 1972.